
This copy is for your personal, non-commercial use only.

If you wish to distribute this article to others, you can order high-quality copies for your colleagues, clients, or customers by [clicking here](#).

Permission to republish or repurpose articles or portions of articles can be obtained by following the guidelines [here](#).

The following resources related to this article are available online at www.sciencemag.org (this information is current as of December 22, 2011):

Updated information and services, including high-resolution figures, can be found in the online version of this article at:

<http://www.sciencemag.org/content/334/6063/1687.full.html>

Supporting Online Material can be found at:

<http://www.sciencemag.org/content/suppl/2011/12/21/334.6063.1687.DC1.html>

This article **cites 31 articles**, 5 of which can be accessed free:

<http://www.sciencemag.org/content/334/6063/1687.full.html#ref-list-1>

Fig. 3B and Table 1, the emission lifetime and quantum yield of the $^3\text{MLCT}$ excited state of $[\text{Co}(\text{pyacac})_3\{\text{Re}(\text{bpy})(\text{CO})_3\}_3]^{3+}$ are identical to that of the GaRe_3 model complex, an observation that indicates a complete absence of reactivity between the charge-transfer excited state of the Re-bpy fragment and the Co^{III} core.

An analysis of the spin-coupled pathways for dipolar energy transfer available in these two systems provides a surprisingly simple explanation for this marked difference in photophysical behavior (Fig. 4). In both compounds, the $^3\text{MLCT}$ excited state has a spin multiplicity of $|S_{\text{D}}^*| = 1$; energy transfer from this state to the $\text{M}(\text{pyacac})_3$ core results in reformation of the singlet ground state of the Re-bpy moiety ($|S_{\text{D}}| = 0$). In the case of $\text{M} = \text{Cr}^{\text{III}}$, the $^4\text{A}_2$ ground state ($|S_{\text{A}}| = 3/2$) creates a spin manifold in the reactant angular momentum space spanning $|S_{\text{R}}| = 1/2, 3/2, \text{ and } 5/2$; this requires coupling to an excited state of the acceptor characterized by $|S_{\text{A}}| = 1/2, 3/2, \text{ or } 5/2$ in order to realize a spin-allowed pathway. Angular momentum conservation is clearly satisfied with the $^4\text{T}_2$ excited state of the Cr^{III} core ($|S_{\text{A}}^*| = 3/2$), as are thermodynamic considerations by virtue of the resonant condition that exists between the Re-bpy emission and the $^4\text{A}_2 \rightarrow ^4\text{T}_2$ absorption. Thus, dipolar energy transfer can proceed through the commonality of $S = 3/2$ states in both the reactants and products, and excited-state quenching of the $^3\text{MLCT}$ emission is observed. Upon replacement of Cr^{III} by Co^{III} , the thermodynamics of energy transfer are essentially unchanged; however, the low-spin d^6 configuration of the $\text{Co}(\text{pyacac})_3$ core fundamentally alters the momentum conservation condition. Specifically, the phosphorescent nature of the $^3\text{MLCT} \rightarrow ^1\text{A}_1$ emission requires coupling to an excited state of the Co^{III} having $|S_{\text{A}}^*| = 1$, not $|S_{\text{A}}^*| = 0$, which defines the $^1\text{A}_1 \rightarrow ^1\text{T}_1$ absorption. Dipolar energy transfer is therefore spin-forbidden for the CoRe_3 assembly, thus giving rise to emission

from the Re-bpy luminophore that is indistinguishable from that of the Ga^{III} model complex.

Although the chemical systems just described were designed specifically to illustrate the principle of angular momentum conservation in dipolar energy transfer, it does not appear to us that this formalism should be limited to energy transfer. In principle, a parallel set of expressions for any chemical reaction could be drafted in which consideration of reactant and product angular momenta serves to differentiate various thermodynamically viable pathways. It seems likely that the issues raised herein will manifest more readily in inorganic rather than organic systems because of the broader array of spin states generally accessible in such compounds; however, we believe that the underlying concepts reflected in this simple formalism and experimentally verified in our study should be generalizable across a wide array of chemical processes.

References and Notes

1. L. D. Landau, E. M. Lifshitz, *The Classical Theory of Fields* (Butterworth-Heinemann, Oxford, 1995).
2. K. K. Rohatgi-Mukherjee, *Fundamentals of Photochemistry* (New Age, New Delhi, 1978).
3. J. R. Lakowicz, *Principles of Fluorescence Spectroscopy* (Springer, New York, ed. 3, 2006).
4. M. A. Baldo *et al.*, *Nature* **395**, 151 (1998).
5. D. Gust, T. A. Moore, A. L. Moore, *Acc. Chem. Res.* **42**, 1890 (2009).
6. E. Wigner, *Nachr. Akad. Wiss. Goettingen Math. Phys.* **K1-2A**, 375 (1927).
7. O. Kahn, *Molecular Magnetism* (Wiley-VCH, New York, 1993).
8. J. H. Moore Jr., *Phys. Rev. A* **8**, 2359 (1973).
9. C. S. Enos, A. G. Brenton, A. R. Lee, *Int. J. Mass Spectrom. Ion Process.* **122**, 361 (1992).
10. R. Burgert *et al.*, *Science* **319**, 438 (2008).
11. B. T. Weldon, D. E. Wheeler, J. P. Kirby, J. K. McCusker, *Inorg. Chem.* **40**, 6802 (2001).
12. C. Achim, E. L. Bominaar, R. J. Staples, E. Münck, R. H. Holm, *Inorg. Chem.* **40**, 4389 (2001).
13. V. W. Manner, A. D. Lindsay, E. A. Mader, J. N. Harvey, J. M. Mayer, *Chem. Sci.* 10.1039/c1sc00387a (2011).
14. J. N. Harvey, *Phys. Chem. Chem. Phys.* **9**, 331 (2007).
15. A. A. Martí *et al.*, *J. Am. Chem. Soc.* **129**, 8680 (2007).

16. A. L. Buchachenko, V. L. Berdinsky, *J. Phys. Chem.* **100**, 18292 (1996).
17. J. D. Kestell, Z. L. Williams, L. K. Stultz, J. P. Claude, *J. Phys. Chem. A* **106**, 5768 (2002).
18. T. Förster, *Discuss. Faraday Soc.* **27**, 7 (1959).
19. T. E. Knight, D. Guo, J. P. Claude, J. K. McCusker, *Inorg. Chem.* **47**, 7249 (2008).
20. Ga^{III} has a closed-shell, d^{10} valence electronic configuration. As such, it is neither redox-active nor does it possess electronic excited states that are energetically available for energy transfer in the visible region.
21. See supporting material at Science Online.
22. J. N. Demas, J. W. Addington, *J. Am. Chem. Soc.* **98**, 5800 (1976).
23. D. Rehm, A. Weller, *Isr. J. Chem.* **8**, 259 (1970).
24. J. P. Claude, T. J. Meyer, *J. Phys. Chem.* **99**, 51 (1995).
25. Y. B. Lei, T. Buranda, J. F. Endicott, *J. Am. Chem. Soc.* **112**, 8820 (1990).
26. L. S. Forster, *Chem. Rev.* **90**, 331 (1990).
27. The extinction coefficients for $[\text{Cr}(\text{pyacac})_3\{\text{Re}(\text{bpy})(\text{CO})_3\}_3]^{3+}$ and the Cr^{III} reference compound $\text{Cr}(\text{phacac})_3$ revealed that $\sim 9\%$ of the incident photons at $\lambda_{\text{pump}} = 375$ nm directly excite the Cr^{III} core; the remaining $\sim 91\%$ are absorbed by the Re-bpy moiety. When the data are scaled accordingly, the observed emission intensity at 80 K is larger than can be accounted for via direct excitation of Cr^{III} by nearly a factor of 10. Further details can be found in fig. S2 and the accompanying text.
28. Estimated from the x-ray structure of $[\text{Ga}(\text{pyacac})_3\{\text{Re}(\text{bpy})(\text{CO})_3\}_3](\text{OTf})_3$ (21).
29. D. L. Dexter, *J. Chem. Phys.* **21**, 836 (1953).

Acknowledgments: We thank G. Blanchard for assistance with the time-correlated single-photon counting emission measurements, and A. Brown and C. McCusker for preliminary spectroscopic measurements on the CoRe_3 assembly. Supported by NSF grant CHE-0911592. Metrical parameters for the structure of compound **3** can be obtained free of charge from the Cambridge Crystallographic Data Centre via www.ccdc.cam.ac.uk/data_request/cif under reference number CCDC 831982.

Supporting Online Material

www.sciencemag.org/cgi/content/full/334/6063/1684/DC1
Materials and Methods
Figs. S1 to S7
Tables S1 to S5
References (30–39)

20 July 2011; accepted 10 November 2011
10.1126/science.1211459

Graphitic Tribological Layers in Metal-on-Metal Hip Replacements

Y. Liao,¹ R. Pourzal,² M. A. Wimmer,³ J. J. Jacobs,^{1,3} A. Fischer,^{2,3} L. D. Marks^{1*}

Arthritis is a leading cause of disability, and when nonoperative methods have failed, a prosthetic implant is a cost-effective and clinically successful treatment. Metal-on-metal replacements are an attractive implant technology, a lower-wear alternative to metal-on-polyethylene devices. Relatively little is known about how sliding occurs in these implants, except that proteins play a critical role and that there is a tribological layer on the metal surface. We report evidence for graphitic material in the tribological layer in metal-on-metal hip replacements retrieved from patients. As graphite is a solid lubricant, its presence helps to explain why these components exhibit low wear and suggests methods of improving their performance; simultaneously, this raises the issue of the physiological effects of graphitic wear debris.

Arthritis, or rheumatism, is the leading cause of disability, affecting an estimated 8.6 million people in the United States as of 2005 (1), with comparable estimates elsewhere. By 2030, the number of American adults

aged 65 and older (the segment of the population with the highest prevalence of arthritis-related disability) will double to ~ 71 million (1). For individuals afflicted with end-stage arthritis of the hip, arthroplasty is the most cost-effective and

clinically successful treatment. Currently, up to three total hip replacement procedures per 1000 inhabitants are performed in countries belonging to the Organisation for Economic Co-operation and Development (2); Germany leads with the largest number of replacements per capita, and the U.S. performs the most procedures overall. As of 2003, $\sim 202,500$ primary total hip replacements were performed annually in the U.S. By 2030, this number is expected to increase by more than 174% to $\sim 572,000$ hip replacements. Arthritis of the hip has an increasingly large public health impact in terms of morbidity, disability, and the cost of disability and treatment. To minimize the impact on the individual patient and society, it

¹Department of Materials Science and Engineering, Northwestern University, Evanston, IL 60201, USA. ²Materials Science and Engineering, University of Duisburg-Essen, Germany. ³Department of Orthopedic Surgery, Rush University Medical Center, Chicago, IL 60612, USA.

*To whom correspondence should be addressed. E-mail: l-marks@northwestern.edu

is imperative that hip replacements are durable, ideally lasting for the extent of the patient's life.

Unfortunately, the materials currently used in hip replacements have limited durability, in large part due to degradation in service. The degradative processes include wear and corrosion, and the products are bioreactive species (micrometer- and nanometer-sized particulate debris and metal ions) that interact with local tissues producing an adverse response that may lead to implant failure and require revision surgery. Another leading cause of total hip replacement failure is postoperative instability (dislocation) (3), which can be minimized by the use of large-diameter femoral heads. This explains the popularity of metal-on-metal (MoM) bearings; for instance, as used in up to 35% of the primary total hip replacement procedures performed in the U.S. MoM bearings are attractive, as they have less wear than metal-on-polyethylene bearings, thereby minimizing debris-associated failures. In addition, their mechanical properties allow thin-walled acetabular components so that large femoral heads can be used. Furthermore, MoM bearings allow hip resurfacing procedures that help to preserve femoral bone stock, which is highly desirable for young patients.

However, there are increasing reports that MoM total hip replacements and surface replacements are not immune to the adverse local tissue responses due to degradation products generated by wear and corrosion that were observed with earlier metal-on-polyethylene bearing couples (4). In April 2010 and February 2011, the regulatory agencies of the UK and the U.S., respectively, issued alerts for MoM hip replacements. These problems seem to be related to specific implant designs as well as nonoptimal positioning, and there are prostheses that have been working successfully in patients for decades (5).

For current MoM bearing hip replacements, which almost always involve austenitic cobalt-chrome-molybdenum (CoCrMo) alloys, a fair amount is known about the metallurgy far below the sliding contact region (microns away) (6). Although the metal plays an important role in

load bearing, there must also be some lubrication mechanism within the human body, as otherwise the wear rates would be prohibitive and severe metal toxicity would be common. Protein in the surrounding fluid is known to play a critical role for MoM replacements (7–10). To date, relatively little is known about the region where active sliding takes place (boundary lubrication), the triboactive region—only that there is a carbon-rich layer. Wimmer *et al.* examined 42 retrieved MoM McKee-Farrar prostheses and reported that more than 80% of them exhibited tribological layers adhered firmly to the surfaces with varying thicknesses (11). The tribological layer was also formed on metal components in simulator tests in bovine serum. It was suggested that this layer was generated during operation in human synovial fluid or bovine serum environments (6, 12). Analyses showed that this tribological layer contained nanoparticles (presumably detached from the substrate) of the metal and a substantial amount of carbon along with possible calcium, oxygen, phosphorus, magnesium, nitrogen, sodium, and chlorine (11, 13, 14). However, relatively harsh methods, which could easily damage carbon-containing compounds, were used to prepare the samples. Other experiments, focusing more on the degradation products with some surface characterization (15, 16), also point toward a tribological layer with different chemistry/properties playing a critical role, plus some chemical changes as lower-molecular weight fragments were observed. It has been commonly assumed (without proof) that the tribological layer is made up of denatured proteins (6, 11, 15–18); that is, proteins that have lost their higher-order structure, with perhaps some minor chemical changes. As such, it would be intrinsically biological in character, similar to lubrication in natural joints. We find, however, that this layer is very different both in form and function, having more in common with lubrication of a combustion engine than lubrication of a natural joint.

Our initial aim was to understand the tribological layer, mainly the embedded metallic nano-

particles, and to look for processes such as carbon segregation to grain boundaries in the near-surface region of the metal. In the process of routine initial characterization by transmission electron microscopy (TEM) of samples thinned with a focused ion beam (FIB), we noticed that electron energy-loss spectra (EELS) showed a strong π^* prepeak, a well-known fingerprint of graphitic carbon (19, 20); high-resolution electron microscope (HREM) imaging experiments suggested a similar conclusion (see figs. S1 and S2).

By itself, this is not sufficient proof of graphitic carbon, as the electron beam in the microscope can change organic materials; one also needs to be concerned about the sample preparation methods. For a definitive test, we need to rule out artifacts from both of these techniques. We therefore used a nanomanipulator inside a dual-beam scanning electron microscopy/FIB system to scrape the tribological layer off of samples retrieved from patients, as shown in Fig. 1. We then generated two control samples (21): (i) dried bovine calf serum, scraped off a substrate made of CoCrMo alloy using FIB under the same conditions (control 1), and (ii) free-standing dried bovine calf serum film on either a copper grid or a silicon membrane (control 2).

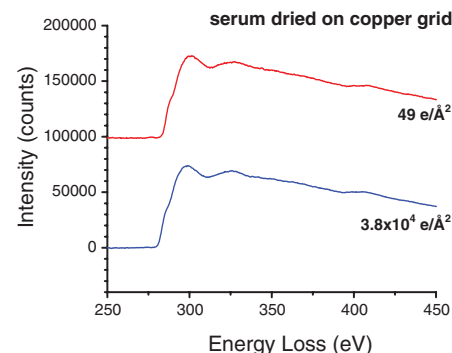
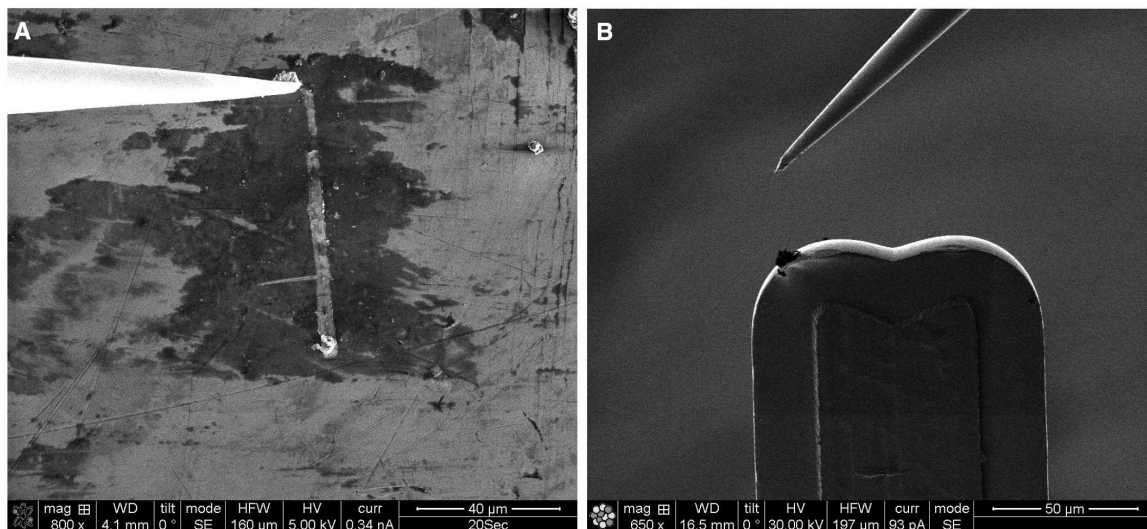


Fig. 2. EELS spectrum of the serum dried on a copper grid for different electron doses, with the $49 \text{ e}/\text{Å}^2$ spectrum offset by 100,000 counts. The change with a dose of $3.8 \times 10^4 \text{ e}/\text{Å}^2$ was minimal.

Fig. 1. (A) The tribological layer (dark region) was scraped off with the use of a tungsten probe in the FIB. (B) The film was attached to a copper TEM grid.



Comparing control 1 with control 2, the carbon peak of the bovine calf serum scraped off using the microprobe in the FIB is essentially the same as that of serum dried directly on a copper grid or a silicon membrane, indicating that specimen preparation in the FIB did not generate any graphitic carbon.

Fig. 3. EELS spectrum of the tribological layer, dried bovine serum, and graphite. The π^* peak is absent in the dried serum but clearly present in the tribological layer, with an sp^2 bonding fraction of 82%.

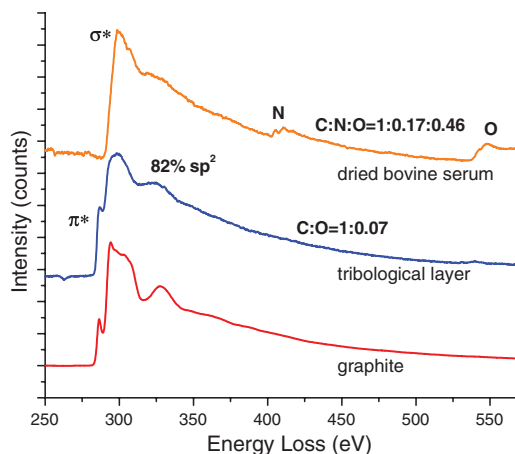


Fig. 4. HREM image of the tribological layer. Short-range ordered graphitic material with a grain size of a few nanometers is present. The inset power spectrum shows that the dominant spacing is ~ 0.34 nm.

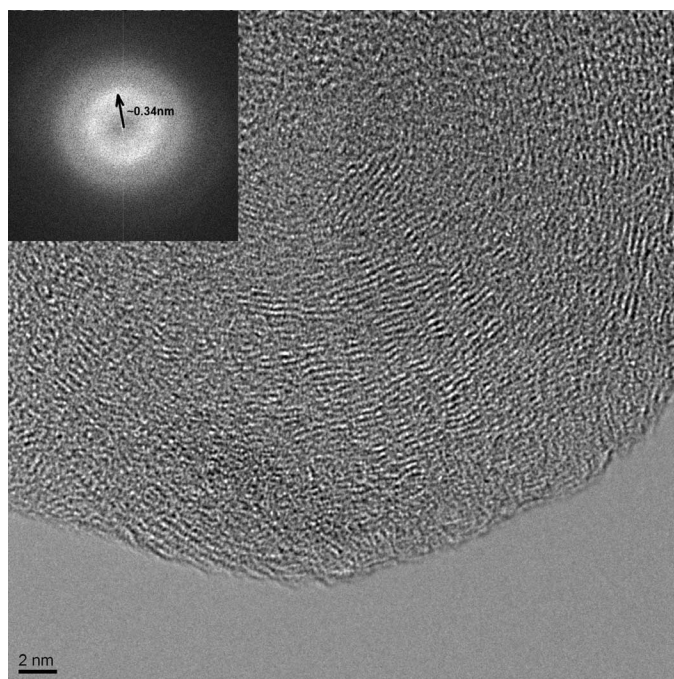
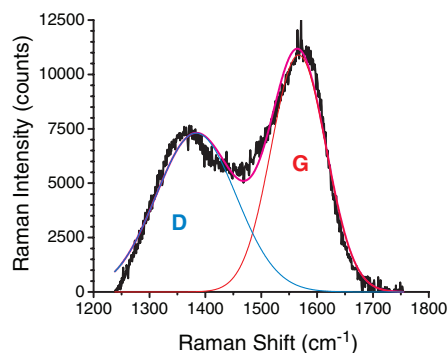


Fig. 5. Raman spectrum of the tribological layer for a CoCrMo hip implant after background subtraction showing the G (red) and D (blue) lines. The data has fit using two Gaussian peaks (purple).



From the control experiments (Fig. 2), we observe that a total dose of $\sim 3.8 \times 10^4$ electrons (e) per \AA^2 does not severely disturb the control samples. It is worth noting that the carbon π^* peak did form under a very high electron dose of $5 \times 10^8 e/\text{\AA}^2$ (fig. S3). A final calibration experiment was to look at the change of the EELS

spectrum as a function of dose for the tribological layers. Supplemental fig. S4 shows that EELS spectra of the tribological layer did not display any discernible change up to a dose of $1.1 \times 10^5 e/\text{\AA}^2$. Thus, the electron dose did not affect the π^* intensity during initial low-magnification TEM imaging and EELS spectrum collection, as would be expected based on work on tribo-induced graphitic material in nearly frictionless carbon (22).

The main experimental results are shown in Fig. 3. A total of three samples [from the first retrieval (21)] analyzed with a dose of $\sim 58 e/\text{\AA}^2$ all showed a clear, strong pre-edge π^* peak as well as low oxygen signals, as did additional samples retrieved from two other patients, one from each (21). In some areas calcium was also present, which we believe came from bone fragments. Using highly ordered pyrolytic graphite as a calibrant, we determined the amount of graphitic carbon as $\sim 82\%$ based on the intensities of the π^* and σ^* peaks (23, 24). The tribological layer did not have any nitrogen, whereas dried bovine calf serum exhibited a strong nitrogen peak. Bovine calf serum dried on a copper grid has experimental C:N:O molar ratios of C:N:O = 1:0.17:0.46 in the EELS data (25), whereas for bovine serum albumin the true ratios are C:N:O = 1:0.27:0.30. The C:O molar ratio in the tribological layer is C:O = 1:0.07. Using the oxygen-integrated edge signal from control 2 as a calibrant, we estimate the atomic percent of oxygen in the tribological material to be 5%.

Figure 4 shows a typical HREM micrograph of the tribological layer along with a power spectrum; every area thin enough for good imaging that was examined showed similar results. Short-range ordered regions are present with a typical size of several nanometers. The spacing of the dominant fringes in the image was measured to be ~ 0.34 nm, confirming that the tribological layer was primarily partially graphitized carbon.

As a secondary confirmation, a Raman spectroscopy result for the tribological layer from the first retrieval is shown in Fig. 5. A broad G line corresponding to the stretch vibration of sp^2 bonding was present, together with a strong D line around 1383 cm^{-1} corresponding to the breathing vibration in disordered sp^2 carbon (26). For comparison, both the G and D lines were absent in the dried serum on a CoCrMo substrate (fig. S5). The G-line position of the tribological layer was 1567 cm^{-1} , slightly shifted from 1580 cm^{-1} of graphite crystal due to the formation of nanocrystallites (27). Using the analysis of carbon structures by Ferrari and Robertson (27), the tribological layer was in between nanocrystalline graphite and amorphous sp^2 carbon [stage 2 in (27)] and was closer to the nanocrystalline side. The fraction of sp^2 bonding was determined from the G-line position to be $>80\%$ based on the plots in (27, 28). Note that the presence of a broad D line also indicated the existence of disordered graphitic carbon. The graphitic domain size (29), L_a , can be calculated from the relative intensities (21, 29, 30) as 4.5 nm, consistent with the HREM observations.

Similar Raman spectra to Fig. 5 indicating a graphitic tribological layer were found at different locations of the first retrieval and from four other retrievals [both wrought and cast alloys (21)], as well as in pin-on-ball tests. Spatially resolved Raman imaging (fig. S6) indicated a definitive correlation between where the graphitic Raman signal came from and where the tribological layer was present. It should be noted that there is extensive literature evidence for a comparable tribological layer in many other retrievals and in simulator tests.

All of the data indicate that the tribological material has a graphitic content similar to partially graphitic carbon. Although we cannot rule out a small impurity of protein in the tribological layer, the fact that there is minimal nitrogen, that a high sp^2 fraction precludes a high hydrogen content, plus the correlation of the Raman and HREM data as to the structure allow us to infer that the fraction of protein is less than 5%, and any protein present should be considered as partially degraded rather than denatured protein.

There are three immediate consequences of this result—the first two are important for orthopedic applications, whereas the other is an issue for concern. The first is that graphite is a standard solid lubricant that is known to perform well in the presence of water (31, 32) and should operate similarly in vivo. In the tribological region, it will serve this purpose, reducing friction as well as corrosion and wear, similar to solid lubricants in an engine. More than just flash-heating or frictional shear of proteins is leading to this layer; instead major chemical changes are taking place that have been hinted at in the degradation product analyses mentioned earlier. Although we do not know the precise mechanism whereby the graphitic material is formed, it is known that many transition metals (here, probably cobalt) will act as catalysts to eliminate water or ammonia from organic materials (33, 34), similar to the well-known coking of heterogeneous catalysts; fresh metal surfaces exposed by wear should be good catalysts. As a crude estimate, the composition of albumin is $C_{3076}H_{4833}N_{821}O_{919}S_{42}$, and eliminating water, ammonia (and hydrogen sulfide) would give a nominal composition of $C_{3076}H_{448}$, which is comparable to typical hydrogenated carbon films used to reduce friction. There is extensive evidence for the formation of graphitic material from other carbon allotropes during sliding, so a conversion from more disordered or amorphous carbon to a graphitic material is expected.

The second consequence is that there is now a design target for improving implants. For instance, one could design to improve adhesion of the graphitic layer to the metal or to promote its formation by changing the alloy composition and thus reducing wear, friction, and corrosion. Biocompatibility of any additives will be an issue, so the problem is not as simple as designing a better alloy.

Lastly, as a caution, wear of this graphitic material is going to lead to the formation of graphitic fragments in the pseudosynovial fluids,

and these can be transported to cells in the nearby regions. The recent finding (4) of a lack of correlation between tissue damage and volumetric wear rate suggests that factors other than cobalt-alloy wear debris may be contributing to adverse tissue reactions. Graphitic carbon may be one such factor; further research is needed.

In summary, we have presented clear evidence that the tribological layer in MoM hip replacements is primarily graphitic carbon. This material forms a layer that reduces friction as well as wear and corrosion and suggests a route for the design of improved implants, although there might be physiological implications associated with graphitic wear debris in patients.

References and Notes

- M. W. Brault, J. Hootman, C. G. Helmick, K. A. Theis, B. S. Armour, *Morb. Mortal. Wkly. Rep.* **58**, 421 (2009).
- Organisation for Economic Co-operation and Development (OECD)/European Union, *Health at a Glance: Europe 2010* (OECD Publishing, Paris, 2010).
- K. J. Bozic et al., *J. Bone Joint Surg. Am.* **91**, 128 (2009).
- D. J. Langton et al., *J. Bone Joint Surg. Br.* **93-B**, 164 (2011).
- S. A. Jacobsson, K. Djerf, O. Wahlström, *Clin. Orthop. Relat. Res.* **329**, 560 (1996).
- M. A. Wimmer, J. Loos, R. Nassutt, M. Heitkemper, A. Fischer, *Wear* **250**, 129 (2001).
- D. Dowson, C. M. McNie, A. A. J. Goldsmith, *Proc. Inst. Mech. Eng. C* **214**, 75 (2000).
- S. C. Scholes, A. Unsworth, *Proc. Inst. Mech. Eng. H* **214**, 49 (2000).
- S. C. Scholes, A. Unsworth, *Proc. Inst. Mech. Eng. H* **220**, 687 (2006).
- A. Unsworth, *Phys. Med. Biol.* **23**, 253 (1978).
- M. A. Wimmer, C. Sprecher, R. Hauer, G. Tager, A. Fischer, *Wear* **255**, 1007 (2003).
- Y. Yan, A. Neville, D. Dowson, *J. Phys. D* **39**, 3206 (2006).
- M. P. Heuberger, M. R. Widmer, E. Zobeley, R. Glockshuber, N. D. Spencer, *Biomaterials* **26**, 1165 (2005).
- M. A. Wimmer et al., *J. Orthop. Res.* **28**, 436 (2010).
- V. K. Maskiewicz, P. A. Williams, S. J. Prates, J. G. Bowsher, I. C. Clarke, *J. Biomed. Mater. Res. B Appl. Biomater.* **94**, 429 (2010).
- H. Mishina, M. Kojima, *Wear* **265**, 655 (2008).

- F. W. Chan et al., *Clin. Orthop. Relat. Res.* **333**, 96 (1996).
- H. McKellop et al., *Clin. Orthop. Relat. Res.* **329**, S128 (1996).
- J. Fink et al., *Solid State Commun.* **47**, 687 (1983).
- S. D. Berger, D. R. Mckenzie, P. J. Martin, *Philos. Mag. Lett.* **57**, 285 (1988).
- Materials and methods are available as supporting material on Science Online.
- A. M'ndange-Pfupfu, O. Eryilmaz, A. Erdemir, L. D. Marks, *Diamond Relat. Mater.* **20**, 1143 (2011).
- J. J. Cuomo, J. P. Doyle, J. Bruley, J. C. Liu, *Appl. Phys. Lett.* **58**, 466 (1991).
- D. L. Pappas et al., *J. Appl. Phys.* **71**, 5675 (1992).
- R. F. Egerton, *Electron Energy-Loss Spectroscopy in the Electron Microscope* (Plenum Press, New York, ed. 2, 1996).
- J. Robertson, *Mater. Sci. Eng. Rep.* **37**, 129 (2002).
- A. C. Ferrari, J. Robertson, *Phys. Rev. B* **61**, 14095 (2000).
- A. C. Ferrari, J. Robertson, *Philos. Trans. R. Soc. London Ser. A* **362**, 2477 (2004).
- F. Tuinstra, J. L. Koenig, *J. Chem. Phys.* **53**, 1126 (1970).
- P. K. Chu, L. H. Li, *Mater. Chem. Phys.* **96**, 253 (2006).
- S. K. Field, M. Jarratt, D. G. Teer, *Tribol. Int.* **37**, 949 (2004).
- B. K. Yen, *Wear* **192**, 208 (1996).
- J. L. Woodman, J. Black, S. A. Jimenez, *J. Biomed. Mater. Res.* **18**, 99 (1984).
- A. Kocijan, I. Milosev, B. Pihlar, *J. Mater. Sci. Mater. Med.* **14**, 69 (2003).

Acknowledgments: This work was funded by the NIH on grant number 1RC2AR058993-01. Northwestern University Atomic and Nanoscale Experimental Center and Biological Imaging Facility are acknowledged for the use of their facilities. We thank K. Shull, K. Wahl, and R. Leapman for invaluable comments and M. Morlock, Hamburg, Germany, for retrievals. The authors have no competing financial interests. As full disclosure of real or potential conflicts of interest, J.J.J. has funding from Zimmer Holdings, Medtronic, and Spinal Motion; consults for Zimmer, Medtronic, Johnson and Johnson, Spinal Motion, and Implant Protection; and has stock options in Implant Protection. A.F. has funding from Zimmer Winterthur and consults for Zimmer, Abbot Vascular, and Ceramtec.

Supporting Online Material

www.sciencemag.org/cgi/content/full/334/6063/1687/DC1
Materials and Methods
Figs. S1 to S6

12 September 2011; accepted 1 November 2011
10.1126/science.1213902

Evidence from Numerical Experiments for a Feedback Dynamo Generating Mercury's Magnetic Field

Daniel Heyner,^{1*} Johannes Wicht,^{2†} Natalia Gómez-Pérez,^{3†} Dieter Schmitt,² Hans-Ulrich Auster,¹ Karl-Heinz Glassmeier^{1,2}

The observed weakness of Mercury's magnetic field poses a long-standing puzzle to dynamo theory. Using numerical dynamo simulations, we show that it could be explained by a negative feedback between the magnetospheric and the internal magnetic fields. Without feedback, a small internal field was amplified by the dynamo process up to Earth-like values. With feedback, the field strength saturated at a much lower level, compatible with the observations at Mercury. The classical saturation mechanism via the Lorentz force was replaced by the external field impact. The resulting surface field was dominated by uneven harmonic components. This will allow the feedback model to be distinguished from other models once a more accurate field model is constructed from MExcury Surface, Space ENvironment, GEochemistry, and Ranging (MESSENGER) and BepiColombo data.

In March 2011, the MExcury Surface, Space ENvironment, GEochemistry, and Ranging (MESSENGER) mission (1) entered orbit

around Mercury. One of its objectives is to explore the planet's magnetic field, which is presumed to be generated by a dynamo operating